Evaluation of Mode Dependent Fluid Damping in a High Frequency Drumhead Microresonator

Santhosh Doreswamy Vishwakarma, Ashok Kumar Pandey, Jeevak M. Parpia, Darren Robert Southworth, Harold G. Craighead, and Rudra Pratap, *Member, IEEE*

***Abstract*— Design of high quality factor (Q) micromechanical resonators depends critically on our understanding of energy losses in their oscillations. The Q of such structures depends on process induced prestress in the structural geometry, interaction with the external environment, and the encapsulation method. We study the dominant fluid interaction related losses, namely, the squeeze film damping and acoustic radiation losses in a drumhead microresonator subjected to different prestress levels, operated in air, to predict its Q in various modes of oscillation. We present a detailed research of the acoustic radiation losses, associated with the 15 transverse vibration modes of the resonator using a hybrid analytical-computational approach. The prestressed squeeze film computation is based on the standard established numerical procedure. Our technique of computing acoustic damping based quality factor Q_{ac} includes calculation of the exact prestressed modes. We find that acoustic losses result in a non-monotonic variation of Q_{ac} in lower unstressed modes. Such non-monotonic variation disappears with the increase in the prestress levels. Although squeeze film damping dominates the net Q at lower frequencies, acoustic radiation losses dominate at higher frequencies. The combined computed losses correctly predict the experimentally measured Q of the resonator over a large range of resonant frequencies. [2013-0035]**

***Index Terms*— Prestressed micro drum resonator, annular plate vibration, high Q resonators, acoustic radiation damping, squeeze film damping, exact modeshape, nonmonotonic acoustic losses.**

I. Introduction

MICROMECHANICAL resonators offer significant advantages over other resonators in terms of size, power consumption [1], CMOS integration [2], and high quality factor, Q [3]. With the advent of micro and nanoelectromechanical systems, there has been rapid development in design and fabrication of sensitive resonant structures that find applications as RF filters [4], mass sensors [5]–[7], pressure sensors [8], and other high-frequency sensors [9]. The sensitivity of these dynamic devices depends on their resonant frequency and quality factor, Q. For devices made of low loss materials, such as silicon, and operating in a fluid medium, such as air, the Q of the device is usually dominated by the fluid interaction dependent losses [10].

For devices oscillating over a fixed substrate at low operating frequencies, the fluid damping is due to a combination of the squeeze-film flow and air-drag [10]–[14]. The squeeze film damping is due to the viscous losses in the sideways motion of the thin air film trapped between the transverse vibrating structure and the fixed substrate [15], [16]. There have been many studies on the squeeze film effect in MEMS and NEMS [10], [13], [14], [17] devices. The findings of these studies indicate that the squeeze film damping reduces with increasing air gap thickness and operating frequency. For large air-gap thickness, the drag losses can dominate the damping in the structure at low frequencies [10] and acoustic damping can dominate the losses at high frequencies [18]. However, for a relatively small air gap, the thin air film, which gives rise to squeeze-film damping at low frequencies [13], behaves like a compressible fluid [14] at higher frequencies. Hence its contribution to net damping reduces drastically at high frequencies. Under such conditions, the damping due to the radiation of acoustic energy from the vibrating surface to the infinitely open surrounding region dominates the loss mechanism [19], [20]. In this paper, we quantify the losses due to acoustic radiation and squeeze film for a conceptually simple structure: an annular plate fixed at its outer edges, suspended over a thin cavity above the fluid substrate and open to the surrounding on the other side (see Fig. 1). We show that the acoustic losses can be reduced by operating the structure at higher harmonics, where the phase difference between the adjacent moving segments at various vibrating modes of the resonator leads to a reduction in radiated energy.

The dynamic motion of the annular plate considered here involves vibration of the device in contact with the surrounding fluid, which is of significant interest in wide range of systems such as a piston that moves in contact with the fluid in a closed cylinder [21], a structure that moves underwater in the ocean [19], the movement of a magnetic disc drive read-head in contact with air [22], vibration of a nano circular drum resonator pressure sensor in contact with

Manuscript received February 2, 2013; revised May 28, 2013; accepted July 14, 2013. This work was supported in part by MCIT CEN phase II, in part by NPMASS under Grant 3.14, and in part by the National Science Foundation under Grants ECCS 1001742 and DMR 1120296. Subject Editor D. Elata.

S. D. Vishwakarma and R. Pratap are with the Department of Mechanical Engineering, Indian Institute of Science, Bengaluru 560 012, India (e-mail: santdmec@mecheng.iisc.ernet.in; pratap@mecheng.iisc.ernet.in).

A. K. Pandey is with the Department of Mechanical Engineering, Indian Institute of Technology, Hyderabad 502205, India (e-mail: ashok@iith.ac.in).

J. M. Parpia and H. G. Craighead are with the Center for Materials Research, Cornell University, Ithaca, NY 14853-2501, USA (e-mail: jmp9@cornell.edu; hgc1@cornell.edu).

D. R. Southworth is with Lehrstuhl für Festkörperphysik, Ludwig-Maximilians-Universität, 80539 Munich, Germany (e-mail: darren.southworth@physik.uni-muenchen.de).

Color versions of one or more of the figures in this paper are available online at http://ieeexplore.ieee.org.

Digital Object Identifier 10.1109/JMEMS.2013.2273803

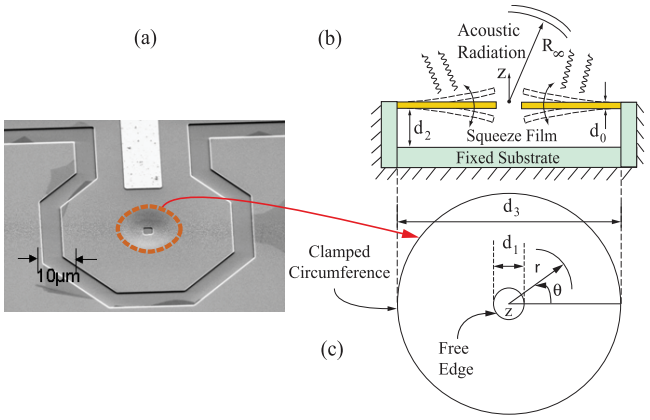

Fig. 1. (a) A picture depicting the prestressed drumhead resonator with a center hole [8]. (b) Depiction of squeeze-film damping and acoustic radiation loss regions, respectively, corresponding to fundamental mode of vibration. (c) Clamped-free circular region with inner radius, $b = \frac{d_1}{2}$, and outer radius, $a = \frac{d_3}{2}$, oscillating near a substrate with an air-gap of d_2.

the surrounding fluid [8], microfluidic devices consisting of a circular membrane [23], and other examples. There are two main effects associated with such systems due to the fluid-structure interaction. First is the "added mass effect", which reduces the effective resonance frequency of the structure. Second is the acoustic radiation loss that affects the quality factor of the vibrating structure. This fluid-structure interaction problem is analyzed numerically using the finite element method or boundary element method for complex domains and analytically for simple domains. Here, we stress on developing an analytical procedure to analyze the acoustic radiation losses on the top side of the vibrating annular plate in several modes of oscillation. The squeeze film damping for the corresponding modes can be readily computed using standard FEM based software, ANSYS [17]. Therefore, our focus is also on developing mathematical formulations for acoustic radiation losses.

Lord Rayleigh [24] was probably the first to study the effect of the mass loading due to the surrounding fluid on a vibrating rigid disk in contact with the fluid. He suggested the idea of an "added mass". This classic problem was then studied by Lamb [19] to investigate the added mass induced change in the first two natural frequencies of a circular plate, fixed along its outer edge and vibrating in contact with a fluid. In addition to the frequency change, Lamb also found the acoustic radiation losses corresponding to those two modes. These results have been validated experimentally by subsequent studies. It is, however, important to note that Lamb's results are based on approximate mode shapes. Revisiting this problem, Amabili *et al*. [25], [26] used the Hankel transform to analyze the added mass effect on the frequency of the structure vibrating in its fundamental and higher modes. However, their study was limited to analysis of the added mass effect on resonators with no prestress. Such fluid-structure interaction effects have recently been analyzed in the context of MEMS/NEMS structures. Unlike the case of macroscale problems, where the surrounding fluid is assumed to be incompressible and inviscid, the experimental validation of Lamb's theory was examined for a microsensor working in the presence of a viscous fluid (water-glycerol mixture) [27]. Experimental results were found to be in good agreement with Lamb's predictions for a less viscous fluid mixture (<10 cP) but differed for fluid mixtures with higher viscosity. The difference was attributed to the viscosity contribution to the added mass effect qualitatively [27] as well as quantitatively [28]. Considering the first approximate mode shape of a circular plate vibrating in contact with the surrounding fluid, Kozlovsky [28] analyzed the effect of viscosity on the natural frequency as well as the quality factor. Recently, Olfatnia *et al*. [18] have compared theoretical and experimental results for analyzing the effect of viscosity of the surrounding fluid on the frequency as well as the quality factor of a circular diaphragm vibrating in its first mode.

Our central interest in the present study is to find acoustic losses and the associated quality factor in various modes of vibration of an annular micromechanical resonator (a MEMS plate) clamped at its outer edge in order to assess the suitability of higher modes to high-Q applications. The annularity of the resonator results from the requirement of an etch hole typically used in the micromachining technique to create a cavity underneath the resonator by dissolving the supporting oxide material starting from the etch hole. Although a pattern with many etch holes could be laid out to penetrate and free up the plate, a central etch hole serves the purpose and creates the simplest resonator structure [8], [29]. The annular resonator is also particularly amenable to analytical treatment for studying acoustic losses [30], [31] and building mathematical models for predicting the Q-factor.

In order to analyze acoustic radiation losses associated with various modes of vibration of the annular plate, we first derive the exact mode shapes of the structure ignoring any effect of the surrounding fluid (air) on the mode shape. We use these mode shapes to study the effect of the surrounding fluid on the associated natural frequencies and the Q-factor. Since the surrounding fluid is air, the effect of "added mass" on the frequencies of the structure is found to be negligible [26]. Hence, it is not considered in the formulation of acoustic damping. The effect of the surrounding air on the Q-factor, however, is significant because of the acoustic radiation losses which is the subject matter of this paper. We extend the analytical approach proposed by Amabili *et al*. [25], [26] to a thin annular plate with prestress (typically present in all thin film micromechanical structures) to find the acoustic losses corresponding to different modes. Finally, we compare our results, first, with Lamb's results for the first two modes, and then with published experimental results [8] for the higher modes of the resonator.

II. Problem Definition

We take a prestressed drumhead resonator with a hole, shown in Fig. 1, which is clamped at its outer edge and separated from the bottom substrate by the air-gap d_2. The air gap comprises a thin film which is present between the substrate and the bottom surface of the annular plate. This thin film is open to the outer surroundings through the hole provided at the center having a diameter d_1 (see Fig. 1(b)).

On the other hand, the upper surface of the plate is in direct contact with the surrounding air which leads to either drag flow damping or acoustic radiation losses. However, drag damping is a low frequency phenomena and is found to be negligible [10], [32], hence, it is not considered in the present study. For the given configuration, under normal operating conditions, there are two types of dominant fluid dissipation mechanisms. The first is termed "squeeze film damping" because of the squeezing of the trapped air film which flows through the etch hole to the surrounding volume above the plate. The second mechanism is due to acoustic radiation damping from the upper surface of the plate. The effect of these two damping mechanisms that contribute in different proportions to the net damping when we consider different resonance modes is analyzed in this paper.

The relevant dimensions and the properties of the resonator and the surrounding air are: the inner diameter $d_1 = 4\ \mu$m, the outer diameter $d_3 = 36.8\ \mu$m, the diameter ratio $\frac{d_1}{d_3} = \frac{b}{a} = 0.1087$, the drum thickness $d_0 = 300$ nm, and the air-gap thickness $d_2 = 572$ nm. The drum is made of polysilicon material with Young's modulus $E = 150$ GPa, Poisson's ratio $\nu = 0.22$ and density $\rho_s = 2330\ \text{kg/m}^3$. The drum oscillates in the surrounding air of density $\rho_f = 1.2\ \text{kg/m}^3$ and viscosity $\mu = 18.3 \times 10^{-6}\ \text{Ns/m}^2$ under constant ambient temperature T = 293 K and pressure $P = 1.013 \times 10^5$ Pa. (Further details of the resonator are available in Southworth *et al*. [8]). The ratio $\frac{d_0}{d_3} \approx 0.008$, suggests that thin plate analysis that includes prestress is sufficient to capture the exact modes of the annular plate. One uncertainty here, however, is the value of the prestress. The residual stress value of 400 MPa mentioned in ref. [8] is for the polysilicon film before patterning and etching. The residual stress in the released resonator structure is not known. Therefore, we carry out modal analysis on the resonator with varying levels of prestress and try to match the experimentally measured frequencies in various modes. The closest match obtained for $\sigma_r = 96$ MPa in all the 15 modes considered makes this value to be the most realistic one for the rest of the analysis.

In the subsequent section, we present the complete mathematical formulation of acoustic radiation damping. On the other hand, since we are using a standard approach to compute the squeeze film damping contribution, we only briefly mention the important steps involved in its computation.

III. Mathematical Modeling of Acoustic Radiation Damping

In this section, we present the mathematical background for computing the acoustic radiation losses due to a vibrating annular plate with free inner edge and fixed outer edge subjected to a radial prestress. The annular plate, with the inner radius, b, and the outer radius, a, in contact with the hemispherical surrounding fluid on its upper surface is shown in Fig. 2.

First, we find the expression for the exact mode shapes of the vibrating annular plate in vacuum. Subsequently, using the same mode shapes, we present the procedure for computing the acoustic radiation losses.

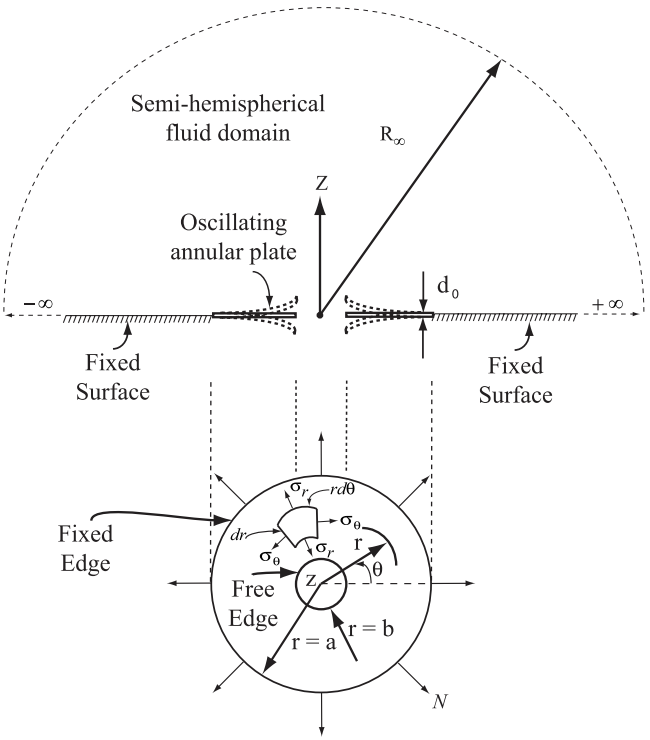

Fig. 2. Schematic of semi-hemispherical fluid domain above the vibrating annular plate with uniform in-plane principal stress state ($\sigma_r = \sigma_\theta$), fixed at its outer edge.

A. Modal Analysis of Annular Plate

The vibration of annular plates with fixed outer boundary is widely analyzed for different applications. Under the assumptions of a thin plate made of isotropic, homogeneous, and linearly elastic material, the equation governing the transverse deflection, $W(r, \theta, t)$, of the plate subjected to radial prestress for undamped, free vibration can be written in polar coordinates as, [33]–[35]

$$\nabla^4 W - \left(\frac{N}{D}\right)\nabla^2 W + \left(\frac{\rho_s d_0}{D}\right)\frac{\partial^2 W}{\partial t^2} = 0, \tag{1}$$

where, $N = \sigma_r d_0$ is the tension per unit length, σ_r is the radial stress, d_0 is the uniform thickness of the plate, $\nabla^2 = \frac{\partial^2}{\partial r^2} + \frac{1}{r}\frac{\partial}{\partial r} + \frac{1}{r^2}\frac{\partial^2}{\partial \theta^2}$ is the Laplacian operator, and $D = \frac{E d_0^3}{12(1-\nu^2)}$ is the flexural rigidity of the plate and ρ_s is the density of the plate. Assuming that the plate vibrates in a normal mode, W can be expressed as,

$$W = w(r, \theta)e^{i\omega t}. \tag{2}$$

Substituting eqn. (2) in eqn. (1) and then rearranging the resulting equation, we get the modal equation as,

$$(\nabla^2 + S^2)(\nabla^2 - \tilde{S}^2)w(r, \theta) = 0, \tag{3}$$

where, $\beta^2 = \frac{\rho_s d_0}{D}\omega^2$ is the frequency parameter, $S^2a^2 = \frac{1}{2}\left(\sqrt{T^4a^4 + 4a^4\beta^2} - T^2a^2\right)$, $\tilde{S}^2a^2 = \frac{1}{2}\left(\sqrt{T^4a^4 + 4a^4\beta^2} + T^2a^2\right)$ and $T = \sqrt{N/D}$. It is noted that for a given tension N, S and $\tilde{S}$ are functions of β only. The modal solution $w(r, \theta)$ can be expressed in terms of Bessel functions [36]

and is given by, [37]

$$w(r,\theta) = \chi(r)\psi(\theta) = [A_{mn}J_n(Sr) + B_{mn}Y_n(Sr) + C_{mn}I_n(\tilde{S}r) + D_{mn}K_n(\tilde{S}r)]\psi(\theta), \tag{4}$$

where, J_n is the Bessel function of the first kind, Y_n is the Bessel function of the second kind, I_n and K_n are the modified Bessel's functions of the first and second kind, respectively.

For the annular plate shown in Fig. 2, the following boundary conditions can be used. At the outer radius $r = a$, $w = \frac{\partial w}{\partial r} = 0$ and at the inner radius $r = b$, the bending moment [38], $M_r = -D\left[\frac{\partial^2 w}{\partial r^2} + \nu(\frac{1}{r}\frac{\partial w}{\partial r} + \frac{1}{r^2}\frac{\partial^2 w}{\partial \theta^2})\right] = 0$ and the shear force [38] $V_r = -D\left[\frac{\partial}{\partial r}\nabla^2 w + \frac{1-\nu}{r^2}\frac{\partial^2}{\partial \theta^2}(\frac{\partial w}{\partial r} - \frac{w}{r})\right] = 0$. On applying these boundary conditions, we get the system of four linear and homogenous equations for the four constants A_{mn}, B_{mn}, C_{mn} and D_{mn} which we list as eqns.(26)–(29) in Appendix A. For a non-trivial solution of these constants, the determinant of the coefficient matrix given by eqn. (38), Appendix C, of the above equations is set to zero, which gives the required characteristic equation governing the frequency constant β. Since the characteristics equation given by eqn. (38) in Appendix C, is difficult to solve analytically, we employ a numerical technique for finding roots in MATLAB to estimate β and then we find S and $\tilde{S}$. The various solutions of β are proportional to the natural frequencies, f, for corresponding modes of vibration. For the given values of S and $\tilde{S}$, the corresponding constants A_{mn}, B_{mn}, C_{mn}, and D_{mn} can be determined by solving the system of linear homogenous equations (26)–(29). Since the equations are homogenous, these constants can be expressed in terms of any one (say D_{mn}). Therefore, expressing the constants A_{mn}, B_{mn}, C_{mn} in terms of D_{mn} and substituting them in eqn. (4), the mode shape can be written as $\frac{w(r,\theta)}{\psi(\theta)} = D_{mn}\tau_{mn}(Sr, \tilde{S}r)$. Normalizing the mode shape based on the normalization condition [26],

$$\int_{b/a}^{1}\left(\frac{w(\alpha,\theta)}{\psi(\theta)}\right)^2 \alpha d\alpha = 1, \tag{5}$$

where, $\alpha = r/a$, we get the expression for D_{mn} as

$$D_{mn} = \frac{1}{\sqrt{\int_{\frac{b}{a}}^{1}\{\tau_{mn}(\alpha Sa, \alpha\tilde{S}a)\}^2 \alpha d\alpha}}. \tag{6}$$

For a particular mode of vibration of the annular plate, the computed D_{mn} from eqn. (6) can be used to determine other constants A_{mn}, B_{mn} and C_{mn} respectively.

For the limiting condition of the annular plate when the radius of the inner hole goes to zero, i.e., a solid plate, we find, following a similar procedure as described above, that Y_n and K_n tend to infinity as r tends to zero [37]. As w is finite at the center of the plate, we must, therefore, set B_{mn} and D_{mn} to be zero. The resulting deflection profile takes the form [35], [37],

$$w(r,\theta) = [A_{mn}J_n(Sr) + C_{mn}I_n(\tilde{S}r)]\psi(\theta). \tag{7}$$

Using the boundary conditions and following a similar procedure as described above, we get the following characteristic equation,

$$J_n(Sa)I_{n+1}(\tilde{S}a)\tilde{S} + I_n(\tilde{S}a)J_{n+1}(Sa)S = 0. \tag{8}$$

For unstressed case, i.e., $\sigma_r = 0$, S and $\tilde{S}$ are equal to $\sqrt{\beta}$. Again, solving the above characteristic equation for β and using the normalization condition, we can obtain expression for values of A_{mn} and C_{mn}.

Most of the fluid structure interaction problems [19] use a polynomial approximation for the mode shapes. However, such approximation introduces errors in estimating the damping from the fluid-structure interaction. In the present analysis, we use exact structural mode shapes for estimating the acoustic radiation losses in different mode shapes.

B. Estimation of Acoustic Radiation Losses

In the previous section, we found the natural frequencies and corresponding mode shapes of the prestressed annular plate vibrating in vacuum. When the plate vibrates while in contact with a surrounding air, the reduction in the modal frequency is found to be negligible [25], [26], [39]. Hence, the added mass effect is not considered in our formulation for estimating the acoustic radiation losses in the surrounding air.

As the annular plate vibrates, a disturbance is created in the fluid adjacent to the plate that causes the wave motion to introduce pressure fluctuations at all points in the fluid domain [40]. Considering the surrounding fluid as irrotational and inviscid at constant ambient mean pressure p_0, temperature T_0 and density ρ_f, the pressure variation about the mean value p_0 and the particle velocity can be found in terms of the velocity potential ϕ through the equation [21], [40]

$$p = -\rho_f \frac{\partial \phi}{\partial t} \text{ and } \upsilon = \nabla\phi. \tag{9}$$

The governing equation for the velocity potential corresponding to small disturbances is given by, [21], [40], [41]

$$\nabla^2\phi - \frac{1}{c_s^2}\frac{\partial^2\phi}{\partial t^2} = 0, \tag{10}$$

where c_s is the speed of acoustic waves in the fluid. The incompressibility condition $\nabla\cdot\upsilon = 0$ leads to the Laplace equation in terms of ϕ, i.e., $\nabla^2\phi = 0$. Therefore, it is sufficient to find the velocity potential field in order to analyze the propagation of waves in the fluid medium.

For the domain shown in Fig. 2, the fixed outer support (i.e., for $r > a$) is assumed to be radially extended to infinity. For the hemispherical fluid domain enclosing the upper surface of the annular plate and the support, along with the Sommerfeld boundary conditions, i.e., velocity and its gradient vanish as $r \to \infty$, the velocity potential can be obtained by solving the wave equation as mentioned above. To find the velocity potential at a generic point P due to an elementary source Ω as shown in Fig. 3, we follow the analysis given by Lamb [19]. Let the position co-ordinates of point P be $(R\sin\xi\cos\psi, R\sin\xi\sin\psi, R\cos\xi)$, and that of Ω on elemental surface area $d\Omega$ in the plane of the resonator be $(r\cos\theta, r\sin\theta, 0)$. The distance r' of the point P from the source position Ω is given by

$$r' = \left\{R^2 - 2Rr\sin\xi\cos(\psi-\theta) + r^2\right\}^{\frac{1}{2}}. \tag{11}$$

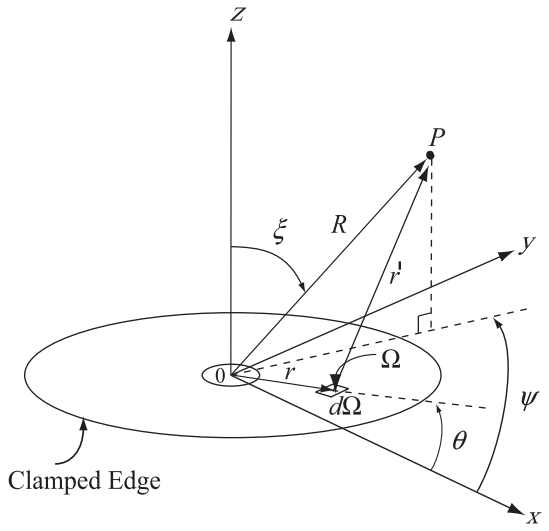

Fig. 3. Generic point P in acoustic far field from the resonator.

Since at the far field point P, $R \gg r$, the expression for r' can be approximated as,

$$r' = \{R - r\sin\xi\cos(\psi - \theta)\}. \tag{12}$$

Assuming that the normal component of the velocity of the fluid at the plate interface is same as that of the plate. The fluid velocity $v_n = \frac{\partial W}{\partial t}$ at point Ω on the upper surface of the annular plate can be written in terms of the mode shape $w(r,\theta)$ defined in section III(A). Since, $W = w(r,\theta)e^{i\omega t}$ and $w(r,\theta) = \chi(r)\psi(\theta) = \chi(r)C\cos n\theta$, we write the normal velocity as,

$$v_n = \frac{\partial W}{\partial t} = i\omega\ w(r,\theta)e^{i\omega t} = A\chi(r)\cos n\theta e^{i\omega t} \tag{13}$$

where, $A = iC\omega$, $\chi(r) = [A_{mn}J_n(Sr) + B_{mn}Y_n(Sr) + C_{mn}I_n(\tilde{S}r) + D_{mn}K_n(\tilde{S}r)]$, ω is the frequency of the vibrating plate. The velocity potential at a distance R from the center of the resonator, or at a distance r' from the elemental surface $d\Omega$ due to the disturbance at Ω is given by, [19], [42]

$$\phi = \frac{1}{2\pi}\int_0^{2\pi}\int_b^a \frac{e^{-ikr'}}{r'}\frac{\partial W}{\partial t}d\Omega. \tag{14}$$

Using the approximation of r' from eqn. (12) and the expression of $\frac{\partial W}{\partial t}$ from eqn. (13), the velocity potential can be rewritten as,

$$\phi = \frac{Ae^{ik(c_st-R)}}{2\pi R}\int_b^a\int_0^{2\pi} e^{ikr\sin\xi\cos(\psi-\theta)} \times \cos n\theta\,\chi(r)r\,dr\,d\theta, \tag{15}$$

where $k = \frac{\omega}{c_s}$ is the acoustic wave number. Using the following property of Bessel functions [22], [43],

$$\int_0^{2\pi} e^{ikrsin\xi\cos(\psi-\theta)}\cos n\theta\,d\theta = 2\pi i^n\cos n\psi\,J_n(kr\sin\xi), \tag{16}$$

the velocity potential can be written as,

$$\phi = \frac{Ai^ne^{ik(c_st-R)}}{R}\cos n\psi \times \int_b^a J_n(kr\sin\xi)\chi(r)r\,dr. \tag{17}$$

From this expression of velocity potential, one can calculate the pressure fluctuation and velocity using eqn. (9). Taking the real part of the velocity potential,

$$\phi_r = \Re\left(\frac{Ai^ne^{ik(c_st-R)}}{R}\right)\cos n\psi \times \int_b^a J_n(kr\sin\xi)\chi(r)r\,dr, \tag{18}$$

corresponding to the real part of the velocity $\frac{\partial W}{\partial t} = \chi(r)\cos(n\theta)\cos(kc_st)$, the intensity of the acoustic wave at any point at distance r' can be written as the product of pressure and particle velocity at that point [21]. The corresponding power radiated across a hemispherical surface of radius R, is obtained by integrating the intensity over the hemispherical fluid domain and can be written as

$$\frac{dE_{\text{flux}}}{dt} = \int_0^{2\pi}\int_0^{\frac{\pi}{2}} -\rho_f\left(\frac{\partial\phi_r}{\partial t}\frac{\partial\phi_r}{\partial R}R^2\sin\xi\right)d\xi\,d\psi. \tag{19}$$

The flux of energy dissipated in the form of sound waves per cycle is given by,

$$\triangle E_{\text{MF}} = \int_0^{\frac{2\pi}{\omega}}\frac{dE_{\text{flux}}}{dt}dt = UA^2. \tag{20}$$

The expression for U is obtained by substituting the velocity potential, ϕ_r, in the power radiated eqn.(19). The parameter U depends on fluid properties, geometric properties, mode shapes and its corresponding frequency of oscillation of the resonator as given below,

$$\begin{aligned} U = &-\rho_f R\int_0^{\frac{\pi}{2}}\left(\int_b^a J_n(kr\sin\xi)\chi(r)r\,dr\right)^2\sin\xi\,d\xi \\ &\times\int_0^{2\pi}\cos^2(n\psi)d\psi\int_0^{\frac{2\pi}{\omega}}\frac{\partial}{\partial t}\left(\Re(i^ne^{ik(c_st-R)})\right) \\ &\times\frac{\partial}{\partial R}\left(\frac{\Re(i^ne^{ik(c_st-R)})}{R}\right)dt. \end{aligned} \tag{21}$$

The input kinetic energy of the plate is given as [19], [26]

$$E_{\text{stored}} = \frac{1}{2}\rho_s d_0\int_0^{2\pi}\int_b^a(\chi(r)A\cos n\theta)^2r\,dr\,d\theta = VA^2. \tag{22}$$

Based on the definition of quality factor [44], we get,

$$Q_{\text{ac}} = \frac{1}{2\zeta} = 2\pi\frac{E_{\text{stored}}}{\triangle E_{\text{MF}}} = 2\pi\frac{V}{U} = \frac{2\pi}{\delta}, \tag{23}$$

where $\delta = U/V$, and is given by,

$$\begin{aligned} \delta = &-\frac{\rho_f}{\rho_s}\frac{R}{d_0}\frac{\int_0^{\frac{\pi}{2}}\left(\int_b^a J_n(kr\sin\xi)\chi(r)r\,dr\right)^2\sin\xi\,d\xi}{\int_b^a\chi^2(r)r\,dr} \\ &\times\int_0^{\frac{2\pi}{\omega}}\frac{\partial}{\partial t}\left(\Re(i^ne^{ik(c_st-R)})\right)\frac{\partial}{\partial R}\left(\frac{\Re(i^ne^{ik(c_st-R)})}{R}\right)dt, \end{aligned} \tag{24}$$

and $\omega = 2\pi f$, where, f being the frequency of the vibrating plate. Although the final expression of the quality factor looks very simple, it requires the computation of δ which is mode dependent. Since the computation of the parameter requires successive differentiation and numerical integration,

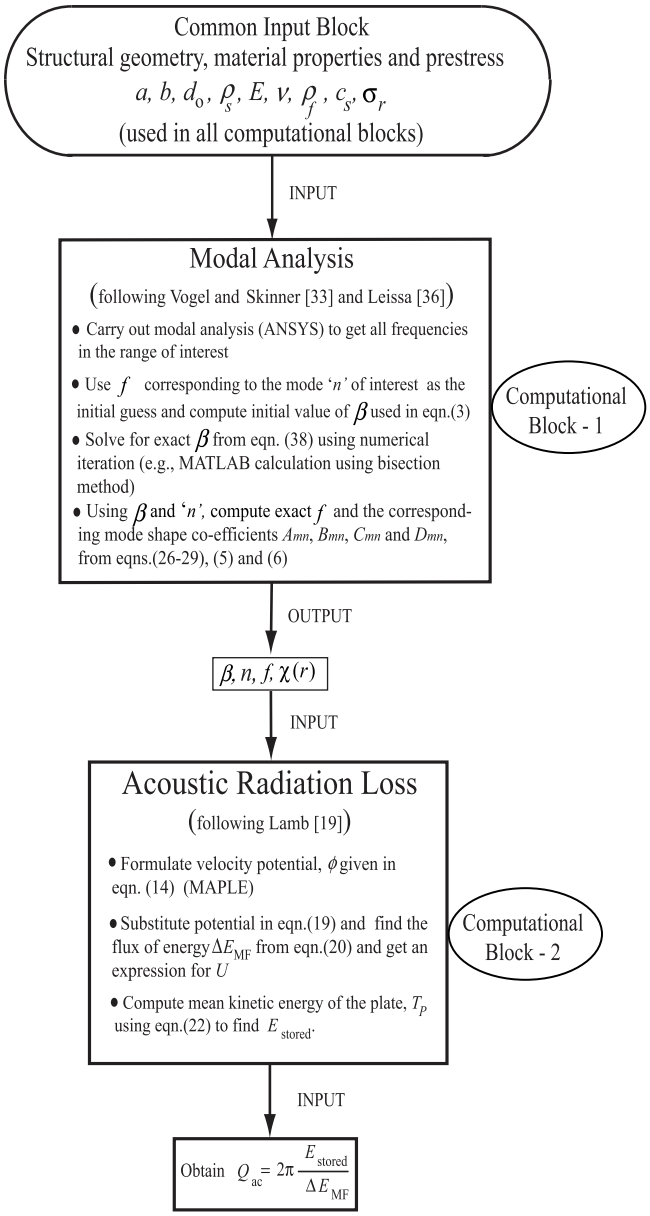

Fig. 4. Flow chart for computing acoustic radiation damping.

we perform these steps in MATLAB and MAPLE. The entire set of calculations is somewhat involved but algorithmic. We, therefore, present the sequence of calculations to be done as a schematic flow chart in Fig. 4.

There are two major computational blocks that we present separately for conceptual clarity. As is evident from Fig. 4, the computation involves some FEM analysis along with computer algebra and general numerics as described in the following section.

C. Steps Involved in Acoustic Damping Calculations

1) *Modal analysis with no fluid*: The goal here is to obtain an analytical expression for the mode shapes of interest and determine the corresponding frequencies for a given prestress σ_r. We do this by the following sequence of steps.
   - Use FEM based modal analysis for the resonator in ANSYS and find numerical values of the natural frequencies f_i of interest.
   - Use the numerically obtained natural frequencies to obtain the initial estimate for the frequency parameter β_i using $f_i = \frac{\beta_i}{2\pi}\sqrt{\frac{Ed_0^2}{12\rho_s(1-\nu^2)}}$. Plug this estimate in the nonlinear algebraic equation for β_i obtained as the characteristic equation for β_i by substituting boundary conditions in eqn.(4), and solve for exact β_i using numerical iteration (MATLAB).
   - Find exact f_i using exact β_i, and by solving the set of homogeneous equations given by boundary conditions on the mode shape, along with the mode normalization condition, determine A_{mn}, B_{mn}, C_{mn}, D_{mn}, and thus the mode shape is given by eqn. (4).
2) *Acoustic radiation loss computation*: We need to evaluate the loss of energy from the resonator to the surrounding fluid in the form of acoustic radiation per cycle of vibration. The computational steps are as follows.
   - Find the velocity potential ϕ derived by Lamb [19] using the exact mode shapes found through the modal analysis.
   - Use the velocity potential to determine the flux of energy radiated in the form of acoustic waves per cycle of oscillation.
   - Compute the mean kinetic energy of the resonator as energy stored.
   - Use the radiated energy and the input energy to find the quality factor Q_{ac} using eqn. (23).

This is the hybrid sequence of analytical and numerical steps that we follow to evaluate the acoustic quality factor for each mode of vibration of the resonator. We can also use the procedure described above to compute the quality factor for an unstressed thin solid circular plate by setting $b = 0$, $\sigma_r = 0$ and $\chi(r) = A_{mn}J_n(\sqrt{\beta}r) + C_{mn}I_n(\sqrt{\beta}r)$.

IV. Squeeze Film Damping Calculations

We use a finite element model for the air film between the resonator structure and the fixed substrate in order to determine the pressure variation in the film and subsequently the squeeze film damping force. The finite element analysis is carried out using ANSYS. The air film is modeled using 2D 4-noded fluid elements with pressure degrees of freedom at each node. The hole effect is modeled using 1D 2-noded fluid element. The fluid elements are coupled to the resonator structure modeled with 8-noded prestress solid elements. The coupled model is shown in Fig. 5. ANSYS solves Reynolds equation in the squeeze film domain taking velocities at structural nodes as the input boundary conditions for the fluid domain on the dynamic interface. ANSYS integrates the pressure field and computes the corresponding stiffness and damping coefficients. The final output is the damping ratio from which we compute Q_{sq}. The Knudsen number, a measure of rarefaction is defined as the ratio of the mean free path, λ_m (65 nm, at ambient pressure and temperature) of air molecules in the air gap at specified macroscopic thermodynamic pressure and temperature to the

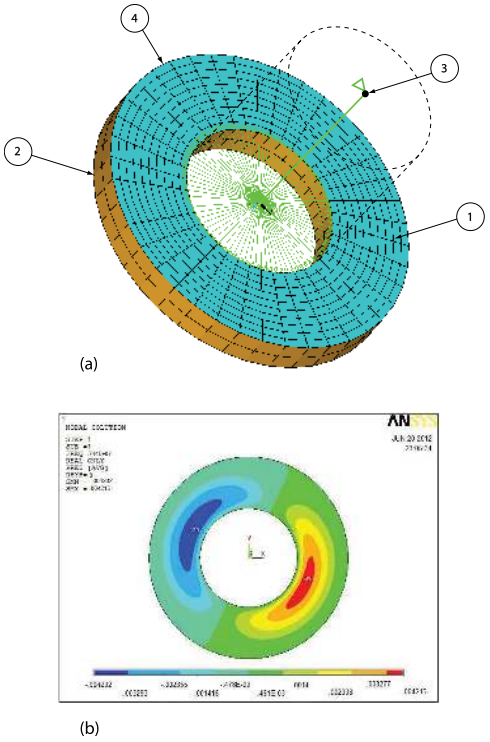

Fig. 5. (a) Finite element model of the resonator using different elements for the solid and fluid regions. ①: 4-noded 2D FLUID136 elements with velocity boundary conditions extracted from modal analysis of adjacent solid elements, ②: 8 noded SOLID185 elements that supports prestress, ③: Ambient pressure specified on the node of FLUID138 elements to capture hole effect and ④: Common nodes of solid and fluid elements that exchange compatible structure-fluid velocities. (b) Pressure contours of squeeze film cavity for a diametral mode.

characteristic flow length, d_2. The Knudsen number of the flow is 0.1136, and falls in the range of transition flow regime [45]. Therefore the rarefaction effect has to be accounted for which is readily done by using an effective viscosity model [45]. We compute μ_{eff} and input this value in ANSYS in order to account for rarefaction. Fig. 5(a) shows the schematic finite element model of the resonator and Fig. 5(b) depicts the squeeze film pressure in the thin air cavity of the drum head resonator.

V. Results and Discussion

In this section, we first discuss the results for quality factor due to acoustic damping and then due to squeeze film damping under prestress effect. Subsequently we find the net Q and compare the results with experimental values obtained by Southworth *et al.* [8]. To do the analysis, we take the dimensions and material properties of the structural and the fluid domains used by Southworth *et al.* [8] in their experimental studies.

A. Acoustic Damping

We first discuss the acoustic damping results for an unstressed solid circular plate oscillating in contact with the surrounding fluid. For the analysis of the solid plate, we simply take the inner radius to be zero, i.e., $b = 0$, $\sigma_r = 0$, and rest of the parameters remain the same.

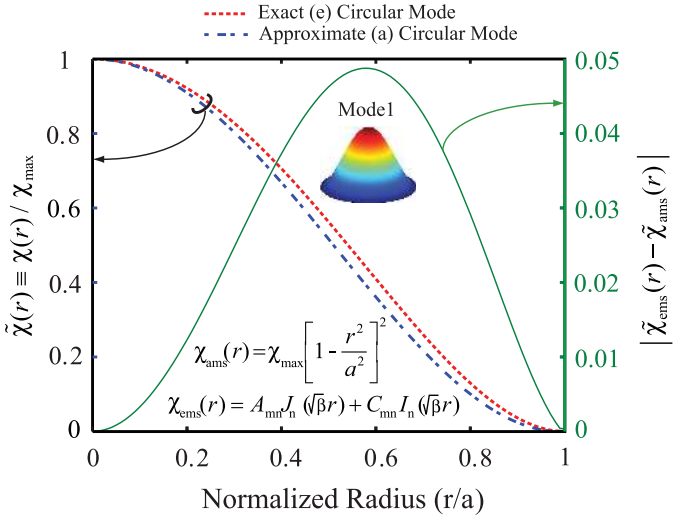

Fig. 6. Normalized circular mode shapes of a clamped and unstressed solid circular plate.

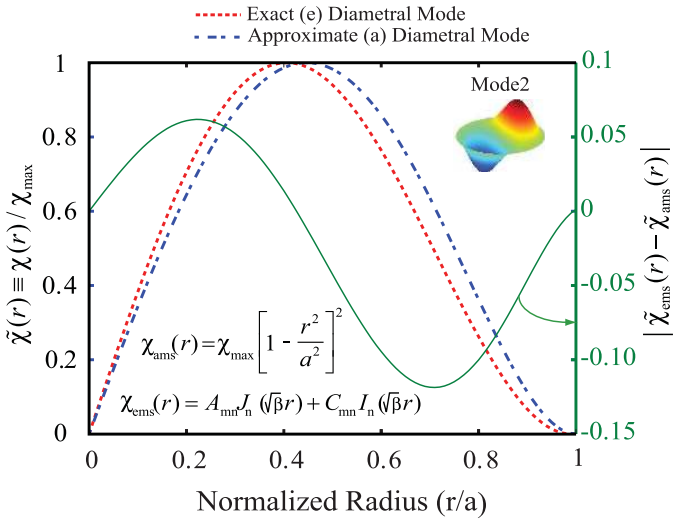

Fig. 7. Normalized diametral mode shapes of a clamped and unstressed solid circular plate.

1) Solid circular plate: We compare the frequency and quality factor based on the exact mode shapes given by eqn. (7) and the approximate mode shapes used by Lamb for the first two modes. Fig. 6 and 7 show the comparison between the normalized exact mode shape (ems) and the normalized approximate mode shape (ams) for the axisymmetric mode with zero nodal circle, i.e., $(m = 0, n = 0)$ and single nodal diameter mode $(m = 0, n = 1)$, respectively. As is evident from these figures, the exact mode shape differs from the approximate one in spatial amplitude variation. The variation is significant enough to cause non-negligible differences in the radiated acoustic power. This is precisely what we see in the computed values of corresponding Q, listed in Table I. The difference in amplitude variation across the plate between the two mode shapes causes very significant change in the corresponding Q. In particular, the approximate mode shape used by Lamb in the second mode overestimates the radiative losses by as much as 42%. This approximation may lead to

TABLE I
QUALITY FACTORS ASSOCIATED WITH EXACT AND APPROXIMATE MODE SHAPES CORRESPONDING TO CIRCULAR AND DIAMETRAL MODES OF UNSTRESSED CIRCULAR SOLID THIN PLATE

m	n	f_{wet} (MHz)	Q_{ems}	Q_{ams}	$\lvert\frac{Q_{\text{ems}}-Q_{\text{ams}}}{Q_{\text{ems}}}\rvert\%$
0	0	3.38	116	100	13
0	1	7.08	233	135	42

even bigger difference when we try to compute the Q's for a prestressed annular plate in the next section.

2) Annular plate: We now consider the annular plate shown in Fig. 2. We intend to compare our analytically computed results with experimental results of Southworth *et al.* [8]. We use the procedure outlined in section III (*A*) to obtain the exact mode shapes of the annular resonator and use these mode shapes to compute the corresponding Q for each mode. In order to estimate the correct value of prestress in the resonator, we compare the experimentally obtained frequencies with the frequencies obtained from the thin annular plate model with varying levels of prestress. We find that the computed frequencies without considering the prestress give lower values as compared to the experimental values listed in Table II. However with a prestress value of 96 MPa, the computed frequencies are found to be the closest in all modes to the experimental results with a maximum percentage error of about 4%. The detailed results are tabulated in Table II. Therefore, we take 96 MPa prestress value for computing acoustic radiation losses. Our focus here is on computing Q_{ac}—the quality factor associated with acoustic radiation losses—and understanding its variation in different modes of vibration. In order to highlight the effect of prestress on Q_{ac}, we plot the computed values of Q_{ac} without prestress and with prestress values of 96 MPa and 400 MPa respectively in Fig. 8. As we can see, the variation in Q_{ac} over the first few modes (<40 MHz) is marked with a local maximum and a minimum for the unstressed case. Beyond this range, however, Q_{ac} increases monotonically. Nevertheless, it is also found that the magnitude of such maximum and minimum reduces as the prestress increases. Figure 8 shows the absence of maximum and minimum corresponding to the prestress level of 400 MPa.

As the mode number increases, the resonator starts behaving like many point sources and addition of more such sources with increasing mode number makes less and less difference to Q_{ac} leading to a somewhat predictable, monotonic and slower increase in Q_{ac}. We point out here that we have ignored any acoustic radiation from the central hole itself in our analysis. The hole area is about 1% of that of the resonator and we find no appreciable fluid volume oscillations in the hole to effect acoustic radiation. The fluid flow in the hole is bulk flow due to squeeze film and the related losses are accounted for in the next section on squeeze film damping.

B. Squeeze Film Damping

For the given device, the squeeze-film region is formed between the drumhead and the fixed bottom substrate as shown in Fig. 1(b). The squeeze-film damping (Q_{sq}^{-1}) corresponding to different modes of annular thin plate subjected to the prestress level of 0, 96 and 400 MPa are computed by following the procedure described in section IV. Figure 9 shows the variation of Q_{sq} with different modes of vibration. It is found that the damping in the fundamental mode is the highest of all the modes because of the large displacement of the fluid in the squeeze-film region. However, as the mode number increases (along with frequency), the damping due to the squeeze film mechanism is reduced and the quality factor increases.

Figure 9 shows the monotonic increase in the squeeze-film based quality factor, Q_{sq}, from 5 to 21 000 calculated for different modal frequencies ranging from 3.4 to 168 MHz for $b/a = 0.1087$ for unstressed case. However, we observe a relatively higher Q_{sq} corresponding to the stress levels of 96 MPa and 400 MPa, respectively. Similar results can also be obtained for other values of b/a. In higher modes of oscillation, the maximum displacement of the fluid decreases and consequently the damping [46] decreases. As is evident from the figure, the Q_{sq} covers a range of five

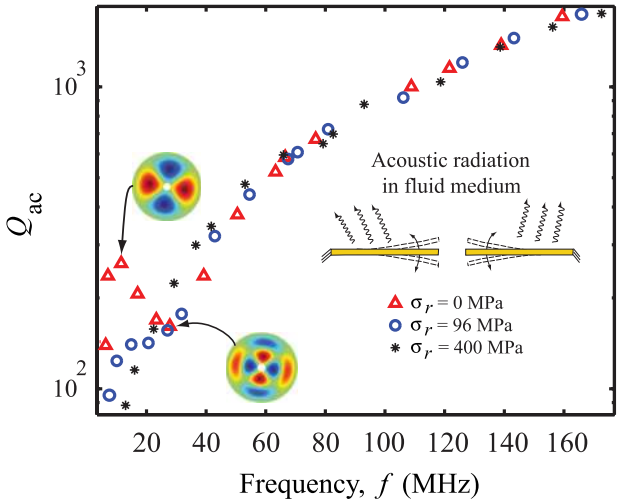

Fig. 8. Calculated acoustic radiation loss based quality factor Q_{ac} variation with resonant modes for prestress levels of 0, 96 and 400 MPa.

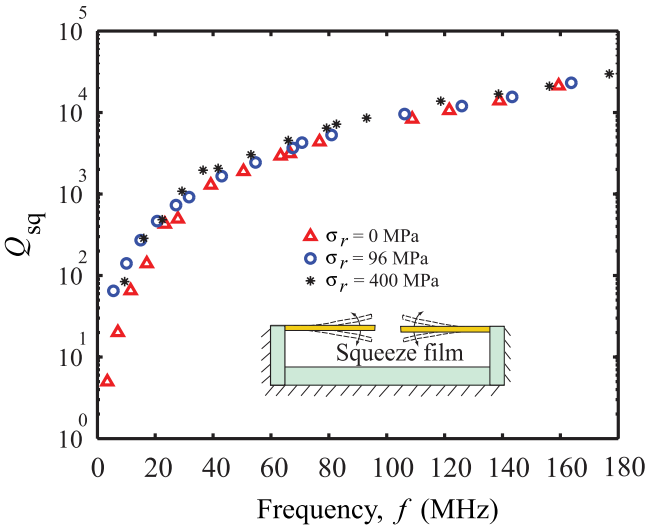

Fig. 9. Calculated squeeze film loss based quality factor, Q_{sq} variation with resonant modes for prestress levels of 0, 96 and 400 MPa.

TABLE II

EXPERIMENTAL AND THEORETICAL COMPARISON OF PRESTRESSED ACOUSTIC Q-FACTORS FOR ANNULAR RESONATOR, CLAMPED AT THE OUTER EDGE (a) AND FREE AT THE INNER EDGE (b) WITH $b/a = 0.1087$

Mode No. (m, n)	Mode Shape	$A_{mn}J_n(Sr) + B_{mn}Y_n(Sr) + C_{mn}I_n(\tilde{S}r) + D_{mn}K_n(\tilde{S}r)$						$f_{96\text{MPa}}$ (MHz)	$f_{\text{Exp.}}$ (MHz)	Quality Factor $Q_{(96\text{MPa})}$
		A_{mn}	B_{mn}	C_{mn}	D_{mn}	$S_{96\text{MPa}}$	$\tilde{S}_{96\text{MPa}}$			
(0, 0)		3.18552	-0.20310	0.01032	0.08404	1.5116e5	3.2257e5	5.52	5.53	83.51
(0, 1)		3.86858	-0.04694	0.00586	0.03150	2.3847e5	3.7158e5	10.04	9.79	123.66
(0, 2)		-4.46571	0.10529	-0.00323	0.13609	3.1189e5	4.22469e5	14.93	14.95	140.10
(0, 3)		-5.04382	0.01525	-0.00172	0.02096	3.8258e5	4.7704e5	20.69	21.08	141.72
(0, 4)		-5.55713	0.00119	-9.2903e-4	0.00166	4.4950e5	5.3222e5	27.12	28.05	156.31
(1, 2)		-5.39951	0.34854	2.5751e-4	0.31933	4.9240e5	5.6892e5	31.75	32.97	177.20
(2, 1)		5.70486	-0.96562	5.4439e-5	1.81419	5.8350e5	6.4937e5	42.95	44.42	320.18
(2, 2)		-6.17613	0.71303	-1.6559e-5	0.40814	6.6544e5	7.2388e5	54.61	53.84	440.27
(2, 3)		-6.62919	0.26692	-5.2537e-6	0.26302	7.45678e5	7.98273e5	67.48	65.34	577.18
(0, 9)		-7.72858	1.6256e-10	-4.2007e-5	2.1306e-10	7.6472e5	8.1609e5	70.75	71.52	607.31
(2, 4)		-7.03412	0.04790	-1.8195e-6	0.05095	8.2148e5	8.6950e5	80.97	77.75	724.04
(0, 12)		-8.79179	3.5157e-14	-6.6091e-6	4.1952e-14	9.4671e5	9.8867e5	106.11	105.10	922.71
(2, 7)		-8.05570	5.2176e-5	-1.0139e-7	5.5791e-5	1.0348e6	1.0733e6	125.92	124.64	1205.45
(1, 11)		-8.79636	1.4897e-11	1.4871e-7	1.6928e-11	1.1063e6	1.1424e6	143.29	143.28	1451.58
(0, 16)		-10.48497	1.5482e-14	-5.6870e-7	1.6737e-14	1.1852e6	1.2190e6	163.80	162.58	1848.005

orders of magnitude over the range of frequencies of interest. Compared to the Q_{ac}, it is easy to see that Q_{sq} dominates at low frequencies (<20 MHz) and plays insignificant role at high frequencies (>40 MHz).

C. Comparison of Net Q With Experimental Results

To compute the total quality factor for the annular thin plate subjected to the prestress of 96 MPa, we use $1/Q_{\text{net}} = 1/Q_{\text{ac}} + 1/Q_{\text{sq}} + 1/Q_{\text{rest}}$. We use this relationship to evaluate the relative contribution of Q_{ac} to Q_{net} (experimentally, Q_{net} is Q_{exp}). Here, we present results from the computation of squeeze-film damping and acoustic radiation damping in the fluid medium under different operating modes characterized by (m, n), compare computed values with experimental results reported earlier [8]. We show that these two damping mechanisms correctly predict the Q of the resonator over a large frequency range. On comparing the net quality factor,

$$Q_{\text{net}} = \left(\frac{1}{Q_{\text{ac}}} + \frac{1}{Q_{\text{sq}}}\right)^{-1}, \tag{25}$$

with the experimental results for $b/a = 0.1087$ [8] as shown in Fig. 10, we find that, at lower harmonics, the squeeze-film effect dominates and for higher harmonics the acoustic damping dominates the Q_{net}. The relative contribution of the two dissipative mechanisms is shown in the form of

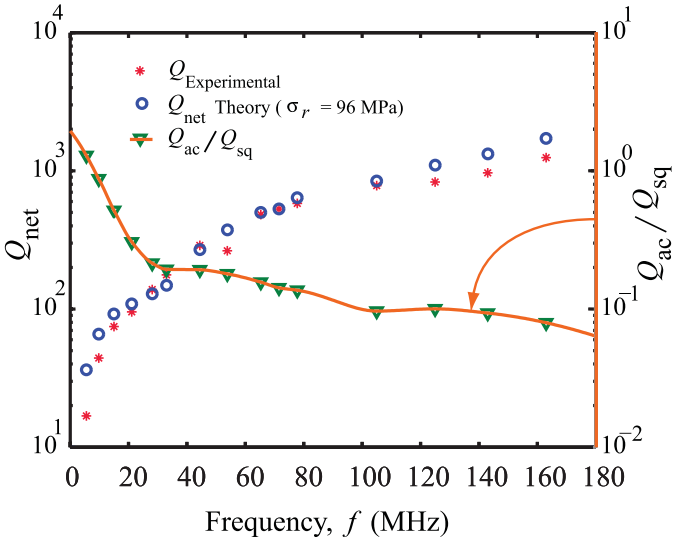

Fig. 10. Comparison of total Q-factor based on squeeze film and acoustic losses for prestress level of 96 MPa, with experimental result [8].

the $Q_{\text{ac}}/Q_{\text{sq}}$ ratio plotted in Fig. 10 using the right axis. This ratio varies over two orders of magnitude, clearly indicating the regions of dominance of one mechanism over the other in various modes. The first three modes (<20 MHz) are dominated by Q_{sq}, the next three modes require both Q_{ac} and Q_{sq} and the rest of the higher modes (>40 MHz) are dominated by Q_{ac}. The results obtained for acoustic radiation losses are interesting because of their non-monotonic variation. The presence of a local maximum and a minimum in Q_{ac} for lower harmonic oscillation modes has significant implications in the design of a MEMS or NEMS resonator. However, such effects can be controlled using pre-stress level. If the design constraints allow other modes of dissipation to be suppressed (e.g., squeeze film damping can be more or less eliminated by increasing the cavity height considerably or by increasing the density of etch holes [47]–[49]) and acoustic losses to be dominant, then one can choose to operate the resonator in the mode corresponding to the local maximum of Q_{ac} to get a high Q device. The non-monotonic behavior of Q_{ac} in the first few modes of the resonator is not intuitive but can be explained by invoking the concept of *acoustic radiation efficiency* [50], [51] which depends on different acoustic radiation parameters such as mode number, intranodal area, intranodal aspect ratio factor as defined in [51]. It is known that different modes of a resonator have different radiation efficiencies, some modes being better radiators than others.

It is evident that the acoustic radiation losses depend on the surrounding fluid medium and the design of the resonator structure. The radiation efficiency of the structure is perhaps best captured by the ratio of the flexural wave number of the structure to the acoustic wave number [50], [51]. The flexural wave number depends on the thickness of the resonator, its flexural rigidity, and its natural frequency. These are not independent design variables. Furthermore, the radiation in higher modes of oscillation depends on the complex interplay of odd and even nodal numbers, intranodal areas, etc., [51]. Thus, in order to make definitive recommendations on design parameters of the resonator, one needs to carry out a separate analysis, perhaps with target Q in mind.

Here, we must point out that we have not considered internal thermoelastic and support losses. In our experience, such losses [29] are typically one to two orders of magnitude smaller than the fluid interaction related losses considered here. The final comparison with experimental results is a clear evidence of the dominance of fluid damping.

VI. Conclusion

We have presented a detailed procedure for computing acoustic damping using exact mode shapes in various modes of vibration of a prestressed annular plate with fixed outer edge. We have also compared the computed Q-factor associated with acoustic radiation for various modes of a micromechanical drum head resonator with published experimental values where the experimental results report the net Q in various modes. We have shown that the contribution of Q_{ac} to the net Q is dominant for higher modes (above the 5$^{\text{th}}$ mode of vibration) and accounts for almost 80% of the net Q. However, the quality factor in the first two modes are governed by squeeze film dissipation mechanism. It is also found that the quality factor based on the squeeze film, Q_{sq}, increases monotonically with the higher modes of vibration for prestress levels of 0, 96 and 400 MPa respectively. However, the variation of acoustic damping based quality factor, Q_{ac}, is quite different over the first few modes in the unstressed state. It is found that Q_{ac} attains a maximum before decreasing and then increasing monotonically. The effect of increase in the prestress diminishes such variations in Q_{ac}, and brings about the monotonic variation in the complete frequency range. However, the magnitude of such effects can be controlled by proper prestress condition. Comparison with published experimental results validates the predictive utility of the calculations, especially for higher modes where acoustic radiation seems to be the dominant constituent of Q. Q_{ac}-like variation is not observed if the net quality factor is dependent both on the squeeze film as well as acoustic damping. The analysis presented in the paper can be extended to different MEMS and NEMS structures to compute acoustic damping.

Appendix A

System of Linear and Homogenous Equations for the Four Constants A_{mn}, B_{mn}, C_{mn} and D_{mn}

$$A_{mn}J_n(Sa)+B_{mn}Y_n(Sa)+C_{mn}I_n(\tilde{S}a)+D_{mn}K_n(\tilde{S}a)=0, \tag{26}$$

$$\begin{aligned}&A_{mn}\left[\tfrac{n}{\tilde{S}a}J_n(Sa)-\tfrac{S}{\tilde{S}}J_{(n+1)}(Sa)\right]\\&+B_{mn}\left[\tfrac{n}{\tilde{S}a}Y_n(Sa)-\tfrac{S}{\tilde{S}}Y_{(n+1)}(Sa)\right]\\&+C_{mn}\left[\tfrac{n}{\tilde{S}a}I_n(\tilde{S}a)+I_{(n+1)}(\tilde{S}a)\right]\\&+D_{mn}\left[\tfrac{n}{\tilde{S}a}K_n(\tilde{S}a)-K_{(n+1)}(\tilde{S}a)\right]=0,\end{aligned} \tag{27}$$

$$\begin{aligned}&A_{mn}F_1(\nu,n,Sb,\tilde{S}b)+B_{mn}F_2(\nu,n,Sb,\tilde{S}b)-C_{mn}F_3(\nu,n,\tilde{S}b)\\&-D_{mn}F_4(\nu,n,\tilde{S}b)=0,\end{aligned} \tag{28}$$

$$\begin{aligned}&A_{mn}\phi_1(\nu,n,Sb,\tilde{S}b)+B_{mn}\phi_2(\nu,n,Sb,\tilde{S}b)-C_{mn}\phi_3(\nu,n,\tilde{S}b)\\&-D_{mn}\phi_4(\nu,n,\tilde{S}b)=0,\end{aligned} \tag{29}$$

$$\begin{vmatrix} J_n(Sa) & Y_n(Sa) & I_n(\tilde{S}a) & K_n(\tilde{S}a) \\ \frac{n}{\tilde{S}a}J_n(Sa) - \frac{S}{\tilde{S}}J_{(n+1)}(Sa) & \frac{n}{\tilde{S}a}Y_n(Sa) - \frac{S}{\tilde{S}}Y_{(n+1)}(Sa) & \frac{n}{\tilde{S}a}I_n(\tilde{S}a) + I_{(n+1)}(\tilde{S}a) & \frac{n}{\tilde{S}a}K_n(\tilde{S}a) - K_{(n+1)}(\tilde{S}a) \\ F_1(\nu, n, Sb, \tilde{S}b) & F_2(\nu, n, Sb, \tilde{S}b) & -F_3(\nu, n, \tilde{S}b) & -F_4(\nu, n, \tilde{S}b) \\ \phi_1(\nu, n, Sb, \tilde{S}b) & \phi_2(\nu, n, Sb, \tilde{S}b) & -\phi_3(\nu, n, \tilde{S}b) & -\phi_4(\nu, n, \tilde{S}b) \end{vmatrix} = 0 \tag{38}$$

where, the functions $F_1, F_2, F_3, F_4, \phi_1, \phi_2, \phi_3$ and ϕ_4 are defined by eqns. (30)-(37) as mentioned on the appendix B.

APPENDIX B

EXPRESSIONS FOR FUNCTIONS F_1, F_2, F_3, F_4, ϕ_1, ϕ_2, ϕ_3 AND ϕ_4

$$F_1(\nu, n, Sb, \tilde{S}b) = \left(\frac{S^2}{\tilde{S}^2}J_n(Sb) - (1-\nu) \times \left[\frac{n(n-1)}{(\tilde{S}b)^2}J_n(Sb) + \frac{S}{\tilde{S}^2 b}J_{(n+1)}(Sb)\right]\right) \tag{30}$$

$$F_2(\nu, n, Sb, \tilde{S}b) = \left(\frac{S^2}{\tilde{S}^2}Y_n(Sb) - (1-\nu) \times \left[\frac{n(n-1)}{(\tilde{S}b)^2}Y_n(Sb) + \frac{S}{\tilde{S}^2 b}Y_{(n+1)}(Sb)\right]\right) \tag{31}$$

$$F_3(\nu, n, \tilde{S}b) = \left(I_n(\tilde{S}b) + (1-\nu) \times \left[\frac{n(n-1)}{(\tilde{S}b)^2}I_n(\tilde{S}b) - \frac{1}{\tilde{S}b}I_{(n+1)}(\tilde{S}b)\right]\right) \tag{32}$$

$$F_4(\nu, n, \tilde{S}b) = \left(K_n(\tilde{S}b) + (1-\nu) \times \left[\frac{n(n-1)}{(\tilde{S}b)^2}K_n(\tilde{S}b) + \frac{1}{\tilde{S}b}K_{(n+1)}(\tilde{S}b)\right]\right) \tag{33}$$

$$\phi_1(\nu, n, Sb, \tilde{S}b) = \frac{S^2}{\tilde{S}^2}nJ_n(Sb) - (\frac{S^3}{\tilde{S}^2}b)J_{(n+1)}(Sb) + \frac{n^2(1-\nu)}{(\tilde{S}b)^2} \times \left[(n-1)J_n(Sb) - (Sb)J_{(n+1)}(Sb)\right] \tag{34}$$

$$\phi_2(\nu, n, Sb, \tilde{S}b) = \frac{S^2}{\tilde{S}^2}nY_n(Sb) - (\frac{S^3}{\tilde{S}^2}b)Y_{(n+1)}(Sb) + \frac{n^2(1-\nu)}{(\tilde{S}b)^2} \times \left[(n-1)Y_n(Sb) - (Sb)Y_{(n+1)}(Sb)\right] \tag{35}$$

$$\phi_3(\nu, n, \tilde{S}b) = nI_n(\tilde{S}b) + (\tilde{S}b)I_{(n+1)}(\tilde{S}b) - \frac{n^2(1-\nu)}{(\tilde{S}b)^2} \times \left[(n-1)I_n(\tilde{S}b) + (\tilde{S}b)I_{(n+1)}(\tilde{S}b)\right] \tag{36}$$

$$\phi_4(\nu, n, \tilde{S}b) = nK_n(\tilde{S}b) - (\tilde{S}b)K_{(n+1)}(\tilde{S}b) - \frac{n^2(1-\nu)}{(\tilde{S}b)^2} \times \left[(n-1)K_n(\tilde{S}b) - (\tilde{S}b)K_{(n+1)}(\tilde{S}b)\right] \tag{37}$$

APPENDIX C

DETERMINANT OF THE COEFFICIENT MATRIX OF EQNS. 26–29

The characteristic equation for frequency parameter β is given by eqn. (38), shown at the top of the page.

ACKNOWLEDGMENT

We acknowledge the fruitful discussions with Prof. V. R. Sonti from Dept. of Mechanical Engineering, Indian Institute of Science on acoustic radiation efficiency and some topics in technical acoustics. The authors thank Robert Anthony Barton from Center for Materials Research, Cornell University for providing essential help with extraction and formatting of data obtained in the original experiment and also for his inputs during the writing of this manuscript. This work was partially supported by MCIT grant CEN phase II, NPMASS grant 3.14, NSF grant ECCS 1001742 and DMR 1120296. The authors would also like to thank both anonymous reviewers for their thoughtful comments and valuable suggestions, specifically on the inclusion of prestress in the analysis.

REFERENCES

[1] C. T.-C. Nguyen, "Frequency-selective MEMS for miniaturized low-power communication devices," *IEEE Trans. Microw. Theory Tech.*, vol. 47, no. 8, pp. 1486–1503, Aug. 1999.

[2] M. K. Zalalutdinov, J. D. Cross, J. W. Baldwin, B. R. Ilic, W. Zhou, B. H. Houston, and J. M. Parpia, "CMOS-integrated RF MEMS resonators," *J. Microelectromech. Syst.*, vol. 19, no. 4, pp. 807–815, Aug. 2010.

[3] V. P. Adiga, B. Ilic, R. A. Barton, I. Wilson-Rae, H. G. Craighead, and J. M. Parpia, "Modal dependence of dissipation in silicon nitride drum resonators," *Appl. Phys. Lett.*, vol. 99, no. 25, pp. 253103-1–253103-5, Dec. 2011.

[4] H. Chandrahalim, D. Weinstein, L. F. Cheow, and S. A. Bhave, "High-κ dielectrically transduced MEMS thickness shear mode resonators and tunable channel-select RF filters," *Sens. Actuators A, Phys.*, vol. 136, no. 2, pp. 527–539, May 2007.

[5] Y. T. Yang, C. Callegari, X. L. Feng, K. L. Ekinci, and M. L. Roukes, "Zeptogram-scale nanomechanical mass sensing," *Nano Lett.*, vol. 6, no. 4, pp. 583–586, Apr. 2006.

[6] K. L. Ekinci, X. M. H. Huang, and M. L. Roukes, "Ultrasensitive nano-electromechanical mass detection," *Appl. Phys. Lett.*, vol. 84, no. 22, pp. 223–225, May 2004.

[7] S. S. Verbridge, R. Ilic, H. G. Craighead, and J. M. Parpia, "Size and frequency dependent gas damping of nanomechanical resonators," *Appl. Phys. Lett.*, vol. 93, no. 1, pp. 013101-1–013101-3, May 2008.

[8] D. R. Southworth, H. G. Craighead, and J. M. Parpia, "Pressure dependent resonant frequency of micromechanical drumhead resonators," *Appl. Phys. Lett.*, vol. 94, no. 21, pp. 213506-1–213506-3, May 2009.

[9] M. Li, H. X. Tang, and M. L. Roukes, "Ultra-sensitive NEMS-based cantilevers for sensing, scanned probe and very high-frequency applications," *Nature Nanotechnol.*, vol. 2, no. 2, pp. 114–120, Feb. 2007.

[10] H. Hosaka, K. Itao, and S. Kuroda, "Damping characteristics of beam-shaped micro-oscillators," *Sens. Actuators A, Phys.*, vol. 49, pp. 87–95, Feb. 1995.

[11] J. J. Blech, "On isothermal squeeze films," *J. Lubricat. Technol.*, vol. 105, pp. 615–20, Oct. 1983.

[12] M. I. Younis and A. H. Nayfeh, "Simulation of squeeze-film damping of microplates actuated by large electrostatic load," *J. Comput. Nonlinear Dyn.*, vol. 2, no. 3, pp. 232–241, Jul. 2007.
[13] A. K. Pandey, R. Pratap, and F. S. Chau, "Influence of boundary conditions on the dynamic characteristics of squeeze films in MEMS devices," *J. Microelectromech. Syst.*, vol. 16, no. 4, pp. 893–903, Aug. 2007.
[14] S. S. Mohite, V. R. Sonti, and R. Pratap, "A compact squeeze-film model including inertia, compressibility, and rarefaction effects for perforated 3-D MEMS structures," *J. Microelectromech. Syst.*, vol. 17, no. 3, pp. 709–723, Jun. 2008.
[15] M. Bao and H. Yang, "Squeeze film air damping in MEMS," *Sens. Actuators A, Phys.*, vol. 136, no. 1, pp. 3–27, May 2007.
[16] M. Bao, H. Yang, H. Yin, and Y. Sun, "Energy transfer model for squeeze-film air damping in low vacuum," *J. Micromech. Microeng.*, vol. 12, no. 3, pp. 341–346, May 2002.
[17] A. K. Pandey and R. Pratap, "Effect of flexural modes on squeeze film damping in MEMS cantilever resonators," *J. Micromech. Microeng.*, vol. 17, no. 12, pp. 2475–2484, Dec. 2007.
[18] M. Olfatnia, Z. Shen, J. M. Miao, L. S. Ong, T. Xu, and M. Ebrahimi, "Medium damping influences on the resonant frequency and quality factor of piezoelectric circular microdiaphragm sensors," *J. Micromech. Microeng.*, vol. 21, no. 4, pp. 045002–045011, Apr. 2011.
[19] H. Lamb, "On the vibrations of an elastic plate in contact with water," *Proc. R. Soc. A, Math. Phys. Eng. Sci.*, vol. 98, no. 690, pp. 205–216, Nov. 1920.
[20] D. W. Greve, I. J. Oppenheim, A. P. Wright, and W. Wu, "Design and testing of a MEMS acoustic emission sensor system," *Proc. SPIE*, vol. 6932, pp. 69321P, Apr. 2008.
[21] L. E. Kinsler, A. R. Frey, A. B. Coppens, and J. V. Sanders, *Fundamentals of Acoustics*. New York, NY, USA: Wiley, 2000, ch. 5, pp. 113–148.
[22] M. Lee and R. Singh, "Analytical formulations for annular disk sound radiation using structural modes," *J. Acoust. Soc. Amer.*, vol. 95, no. 6, pp. 3311–3323, Jun. 1994.
[23] R. Pratap, S. S. Mohite, and A. K. Pandey, "Squeeze film effects in MEMS devices," *J. Indian Inst. Sci.*, vol. 87, no. 1, pp. 75–94, Mar. 2007.
[24] J. W. S. L. Rayleigh, *The Theory of Sound*, vol. 1. New York, NY, USA: Dover, 1945, p. 480.
[25] M. Amabili and M. K. Kwak, "Free vibrations of circular plates coupled with liquids: Revising the Lamb problem," *J. Fluids Struct.*, vol. 10, no. 7, pp. 743–761, Oct. 1996.
[26] M. Amabili, G. Frosali, and M. K. Kwak, "Free vibrations of annular plates coupled with fluids," *J. Sound Vibrat.*, vol. 191, no. 5, pp. 825–846, Apr. 1996.
[27] C. Ayela and L. Nicu, "Micromachined piezoelectric membranes with high nominal quality factors in Newtonian liquid media: A Lamb's model validation at the microscale," *Sens. Actuators B, Chem.*, vol. 123, pp. 860–868, Nov. 2007.
[28] Y. Kozlovsky, "Vibration of plates in contact with viscous fluid: Extension of Lamb's model," *J. Sound Vibrat.*, vol. 326, nos. 1–2, pp. 332–339, Sep. 2009.
[29] V. P. Adiga, B. Ilic, R. A. Barton, I. Wilson-Rae, H. G. Craighead, and J. M. Parpia, "Approaching intrinsic performance in ultra-thin silicon nitride drum resonators," *J. Appl. Phys.*, vol. 112, no. 6, pp. 064323-1–064323-6, Sep. 2012.
[30] M. C. Junger and D. Feit, *Sound, Structures, and Their Interaction*. Cambridge, MA, USA: MIT Press, 1972.
[31] W. P. Rdzanek, "The sound power of an individual mode of a clamped-free annular plate," *J. Sound Vibrat.*, vol. 261, no. 5, pp. 775–790, Apr. 2003.
[32] W. Zhang and K. Turner, "Frequency dependent fluid damping of micro/nano flexural resonators: Experiment, model and analysis," *Sens. Actuators A, Phys.*, vol. 134, no. 2, pp. 594–599, Mar. 2007.
[33] S. M. Vogel and D. W. Skinner, "Natural frequencies of transversely vibrating uniform annular plates," *J. Appl. Mech.*, vol. 32, no. 4, pp. 926–931, Dec. 1965.
[34] P. N. Raju, "Vibrations of annular plates," *J. Aeronaut. Soc. India*, vol. 14, no. 2, pp. 37–52, May 1962.
[35] J. S. Rao, *Dynamics of Plates*. New York, NY, USA: Marcel Dekker, 1999, chs. 3–4, pp. 43–148.
[36] A. W. Leissa, *Vibration of Plates*, vol. 160. Washington, DC, USA: NASASP, 1969, pp. 22–23.
[37] G. N. Watson, *A Treatise on the Theory of Bessel Functions*. New York, NY, USA: Cambridge Univ. Press, 1944, chs. 3–5, pp. 38–132.
[38] S. P. Timoshenko and S. Woinowsky-Krieger, *Theory of Plates and Shells*. Auckland, New Zealand: McGraw-Hill, 1959, ch. 9, pp. 282–324.
[39] M. K. Kwak and K. C. Kim, "Axisymmetric vibration of circular plates in contact with fluid," *J. Sound Vibrat.*, vol. 146, no. 3, pp. 381–389, May 1991.
[40] H. Lamb, *The Dynamical Theory of Sound*. London, U.K.: Arnold, 1931, ch. 7, pp. 200–286.
[41] E. J. Skudrzyk, *The Foundations of Acoustics—Basic Mathematics and Basic Acoustics*. New York, NY, USA: Springer-Verlag, 1971, ch. 23, pp. 489–511.
[42] J. W. S. L. Rayleigh, *The Theory of Sound*, vol. 2. New York, NY, USA: Dover, 1945, ch. 14, pp. 97–148.
[43] E. J. Skudrzyk, *The Foundations of Acoustics—Basic Mathematics and Basic Acoustics*. New York, NY, USA: Springer-Verlag, 1971, ch. 26, pp. 593–640.
[44] S. S. Rao, *Mechanical Vibrations*. 2nd ed. New York, NY, USA: Addison-Wesley, 2011, chs. 2–3, pp. 6–174.
[45] T. Veijola, "End effects of rare gas flows in short channels and in squeezed-film dampers," in *Proc. 5th Int. Conf. Model. Simul. Microsyst.*, Apr. 2001, pp. 104–107.
[46] A. K. Pandey and R. Pratap, "A semi-analytical model for squeeze-film damping including rarefaction in a MEMS torsion mirror with complex geometry," *J. Micromech. Microeng.*, vol. 18, pp. 105003-1–105003-12, Aug. 2008.
[47] G. D. Pasquale, T. Veijola, and A. Soma, "Modelling and validation of air damping in perforated gold and silicon MEMS plates," *J. Micromech. Microeng.*, vol. 20, pp. 015010-1–015010-12, Nov. 2010.
[48] D. Homentcovschi and R. N. Miles, "Analytical model for viscous damping and the spring force for perforated planar microstructures acting at both audible and ultrasonic frequencies," *J. Acoust. Soc. Amer.*, vol. 124, no. 1, pp. 175–181, Jul. 2008.
[49] S. S. Mohite, V. H. Kesari, and R. Pratap, "Analytical solutions for the stiffness and damping coefficients of squeeze films in MEMS devices with perforated back plates," *J. Micromech. Microeng.*, vol. 15, no. 11, pp. 2083–2092, Nov. 2005.
[50] F. J. Fahy and P. Gardonio, *Sound and Structural Vibration: Radiation, Transmission and Response*, 2nd ed. New York, NY, USA: Academic, 2007, p. 151.
[51] C. E. Wallace, "Radiation resistance of a rectangular panel," *J. Acoust. Soc. Amer.*, vol. 51, no. 3B, pp. 946–952, Jul. 1972.

Santhosh D. Vishwakarma received the B.E. degree in mechanical engineering from the Bangalore Institute of Technology, Bengaluru, India, in 2002, and the M.Tech. degree in machine design from the B.M.S. College of Engineering, Bengaluru, in 2006. He is currently pursuing the Ph.D. degree in the Department of Mechanical Engineering and Supercomputer Education Research Centre, Indian Institute of Science, Bengaluru.

He was a Project Engineer with Hindustan Aeronautics Ltd., Bengaluru, from 2002 to 2003. He had a year of exposure in the Smart Materials and Structure Group at the National Aerospace Laboratories, Bengaluru, during his master's project. His current research interests include multiscale modeling (FEM, Monte Carlo), MEMS/NEMS design, analysis and its related damping mechanisms. He has received a gold medal for his academic excellence in his master's degree.

Ashok K. Pandey received the B.E. degree in mechanical engineering from the Bhilai Institute of Technology, Durg, India, in 2001, and the M.S. and Ph.D. degrees in mechanical engineering from the Indian Institute of Science, Bengaluru, India, in 2003 and 2007, respectively.

He was a Research Associate with the Department of Mechanical Engineering from 2007 to 2008. He was a Post-Doctoral Fellow with the Technion-Israel Institute of Technology, Haifa, Israel, from 2008 to 2010. He is currently an Assistant Professor with the Department of Mechanical Engineering, Indian Institute of Technology, Hyderabad, India. His current research interests include linear and nonlinear vibration, modeling and simulation of vehicle dynamics, micro and nanomechanical systems, microfluidics and nanofluidics, mechanics involved with carbon nanotubes, and quantum nanoelectromechanical systems. He was conferred with the Hetenyi Award by the Society of Experimental Mechanics in 2010.

Jeevak M. Parpia received the B.S. degree from the Illinois Institute of Technology, Chicago, IL, USA, in 1973, and the M.S. and Ph.D. degrees in experimental physics from Cornell University, Ithaca, NY, USA, in 1979.

He was an Assistant and Associate Professor with Texas A&M University, College Station, TX, USA, from 1979 to 1986, before moving back to Cornell's Physics Department. He is currently a Professor and Chair of the Department of Physics. His current research interests include the physics of 3He, MEMS and NEMS structures adapted for sensing, mechanics and opto mechanics of graphene. He is a Fellow of the American Physical Society.

Darren R. Southworth received the B.S. degree in engineering physics from the University of Maine, Orono, ME, USA, in 2005, and the Ph.D. degree from Cornell University, Ithaca, NY, USA, in 2010.

He is currently a Post-Doctoral Fellow at the Lehrstuhl für Festkörperphysik, Ludwig-Maximilians-Universität, Munich, Germany, focusing on fundamental investigation of nanomechanical systems.

Harold G. Craighead received the B.S. (Hons.) degree in physics from the University of Maryland, College Park, MD, USA, in 1974, and the Ph.D. degree in physics from Cornell University, Ithaca, NY, USA, in 1980. From 1979 to 1984, he was a Technical Staff Member with the Device Physics Research Department, Bell Laboratories, Murray Hill, NJ, USA. In 1984, he joined Bellcore, Red Bank, NJ, USA, where he formed and managed the Quantum Structures Research Group. He joined the faculty of Cornell University as a Professor in the School of Applied and Engineering Physics in 1989. From 1989 to 1995, he was the Director of the National Nanofabrication Facility, Cornell University. He was the Director of the School of Applied and Engineering Physics from 1998 to 2000 and the Founding Director of the Nanobiotechnology Center from 2000 to 2001. He served as an Interim Dean of the College of Engineering from 2001 to 2002, after which he returned to the Nanobiotechnology Center as a Co-Director. He has been a pioneer in nanofabrication methods and the application of engineered nanosystems for research and device applications. His recent research activity includes the use of nanofabricated devices for biological applications. His research continues to involve the study and development of new methods for nanostructure formation, integrated fluidic/optical devices, nanoelectromechanical systems, and single molecule analysis.

Dr. Craighead was elected to the National Academy of Engineering in February 2007. According to the academy, Craighead, director of Cornell's Nanobiotechnology Center, was selected for "contributions to the fabrication and exploitation of nanostructures for electronic, optical, mechanical and biological applications". He has been a pioneer in using nanostructures as tools in biological research. His research group has created devices that can detect and identify single bacteria and viruses, nanoscale gas sensors and nanofluidic devices that can separate, count and analyze individual DNA molecules.

Rudra Pratap (M'07) received the B.Tech. degree from the Indian Institute of Technology (IIT), Kharagpur, India, in 1985, the M.S. degree in mechanics from the University of Arizona, Tucson, AZ, USA, in 1987, and the Ph.D. degree in theoretical and applied mechanics from Cornell University, Ithaca, NY, USA, in 1993.

From 1993 to 1996, he was with the Sibley School of Mechanical and Aerospace Engineering, Cornell University. In 1996, he was with the Indian Institute of Science, Bengaluru, India. From 1997 to 2000, he was an Adjunct Assistant Professor at Cornell University. He was an Invited Professor at the Ecole Polytechnique Federal de Lausanne, Lausanne, Switzerland, from 2004 to 2005. He is currently the Chairperson of the Center for Nano Science and Engineering and an Associate Faculty Member with the Department of Mechanical Engineering, Indian Institute of Science. His current research interests include MEMS design, computational mechanics, nonlinear dynamics, structural vibration, and vibroacoustics. He is a member of the Institute of Smart Structure and System and is on the Editorial Board of the *Journal of Computers, Materials and Continua* and the *Journal of Shock & Vibration*.